Electronic Supplementary Material (ESI) for Environmental Science: Processes & Impacts.

Supplemental Information

Chemical and Physical Properties of Organic Mixtures on Indoor Surfaces during HOMEChem

Rachel E. O'Brien,[1] Ying Li,[2] Kristian J. Kiland,[3] Erin F. Katz,[4†] Victor W. Or,[5] Emily Legaard, Emma Q. Walhout,[1] Corey Thrasher,[1] Vicki H. Grassian,[5,6] Peter F. DeCarlo,[7] Allan K. Bertram,[3] Manabu Shiraiwa[2]

[1]Department of Chemistry, William & Mary, Williamsburg, VA, 23185, USA

[2] Department of Chemistry, University of California, Irvine, CA, 92697, USA

[3]Department of Chemistry, University of British Columbia, Vancouver, British Columbia V6T 1Z1, Canada

[4]Department of Chemistry, Drexel University, Philadelphia, PA 19104, USA

[5]Department of Chemistry and Biochemistry, University of California San Diego, La Jolla, California 92093, USA

[6]Scripps Institution of Oceanography and Department of Nanoengineering, University of California San Diego, La Jolla, California 92093, USA

[7]Department of Environmental Health and Engineering, Johns Hopkins University, Baltimore, MD, 21218, USA

[†]Now at: Department of Chemistry, UC Berkeley, Berkeley CA, 94720, USA

Materials and Methods

MS Analysis:

For comparison of HR-AMS data sets, the dot product between the spectra was calculated using:

$$Dot\ product = \frac{\sum(I_{extract} \times I_{online})}{\sqrt{\sum I_{extract}^{2} \times \sum I_{online}^{2}}}$$

where $I_{extract}$ and I_{online} are the intensities of the ions in the offline HR-AMS and the online HR-AMS mass spectra, respectively. Both mass spectra were normalized to a sum of one and the mass range was used to *m/z* 100.

Both AMS mass spectra shown in Figure 1 are C, H, and O only containing ions. Previous work has demonstrated the presence of siloxanes in aerosol particles during HOMEChem.[1] Here, no siloxanes were observed in the offline-AMS mass spectrum, possibly because of dominance of the COA mass for the cumulative sample, or the limited solubility of the siloxanes in water. The FT-ICR samples showed peaks with isotope distributions consistent with siloxanes in the mass range of approximately 1,000-1,400 *m/z* (data not shown). However, the same peaks were also observed in the field blank. This suggests that the siloxanes were prevalent enough to contaminate the field blank, and that they likely have reasonably high ionization efficiency in positive ion mode for electrospray ionization. We do not expect that the siloxanes observed in the FT-ICR data are from o-rings as no o-rings are used in the extractor or in the instrument. Since the FT-ICR data is not quantitative and the peaks were observed in the blank, they were not considered in this analysis.

Viscosity measurements:

The viscosity of the HOMEChem extract samples was measured using the poke-flow technique.[2–7] First, the HOMEChem extract was dissolved in 1 mL of methanol, and then 1 μL droplets of the resulting solution were pipetted onto hydrophobic glass slides (12 mm glass slides coated with CYTONIX, FluoroPel 800). The hydrophobic slides were then placed in a laminar flow hood under room conditions to allow the methanol to evaporate over the period of 1.5 hours to > 5 days (the results were not sensitive to this range of evaporation times). After the methanol evaporated, the sample formed close to a spherical cap geometry on the fluorinated slides. After evaporation, the fluorinated slides were placed in a flow cell (Fig. S1) mounted above an inverted optical microscope (AmScope, ME1400TC-INF). The relative humidity (RH) in the flow cell was controlled by controlling the RH of the carrier gas. The RH was calculated from measurements of the temperature and dewpoint of the carrier gas. The temperature was measured using a thermocouple (OMEGA, HH-200a) attached to the metal body of the flow cell. The dewpoint was measured using a hygrometer (General Eastern, optical dewpoint sensor 1311DR) placed upstream of the flow cell.

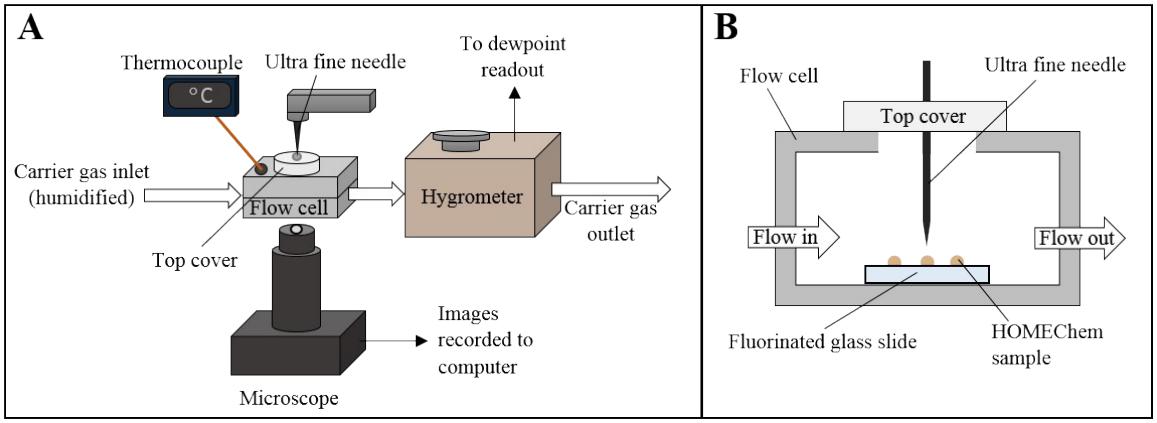

Figure S1. Panel A shows a schematic of the poke-flow apparatus. Panel B shows the sample slide placed inside the flow cell.

An ultra-fine tungsten needle (Roboz Surgicial Instruments Co.) with an oleophobic coating (CYTONIX, OilSlip 110) was used to poke the sample. After poking the sample, a half torus geometry was formed. If given enough time, the half torus geometry returned to the near spherical cap geometry to minimize the surface energy of the system. Images of the sample during the poke-flow experiments were recorded using a microscope camera (AmScope, MA1000) attached to a computer. From the images, we determined the experimental flow time ($\tau_{exp,\ flow}$), defined as the time for the area of hole in the half torus geometry to reach a value of $1/4A_0$, where A_0 is the initial area of the hole after poking.

For the HOMEChem extract samples, the samples flowed rapidly, and the half torus geometry quickly returned to a near spherical-cap geometry (see Movie S1 as an example). From the images we estimated that $\tau_{exp,\ flow}$ was less than 0.4 s, which is roughly the time it took to remove the needle from the sample after poking. For contrast, Movie S2 shows an example of images recorded in a poke-flow experiment for sucrose-water particles with viscosity of $2.75 \times 10^4 - 1.49 \times 10^5$ Pa s at an RH value of 49%. For this case, $\tau_{exp,\ flow}$ was 32.5

s.

The upper limit to the experimental flow times were converted into an upper limit to the viscosity using fluid dynamic simulations.[2] The simulations were carried out with COMSOL Multiphysics (v5.4). The half-torus geometry was used in the simulations with dimensions matching the experiments. The simulations used the Microphysics Module within COMSOL and a laminar two-phase flow with moving mesh. In the simulations, the viscosity was adjusted until the inner area of the simulated half-torus geometry, $A_{0,model}$, reached a value of $1/4A_{0,model}$ in the same amount of time as $\tau_{exp,\ flow}$. Since 0.4 s is an upper limit to the $\tau_{exp,\ flow}$, the viscosity from the simulations will be upper limits to the true viscosity.

For the simulations, values for the density of the material, surface tension of the material, contact angle of the material, and the Navier slip length are needed. Values used in the simulations are shown in Table S1.

Table S1. Input parameters for poke-flow COMSOL simulations to obtain upper limits of viscosity.

Input parameter	Value used in upper limit viscosity simulation
Density	915.7 kg/m^3
Surface tension	0.1346 N/m
Navier slip length	1000 nm
Contact angle	52.8° - 59.8°

For the contact angle, we used values based on measurements with a confocal laser scanning microscope. For the density, we used the density of soy oil at 20 °C.[8] The simulated viscosities were not sensitive to this parameter. For the surface tension, we use the surface

tension of maltopentose (0.1346 N/m).[9] For comparison, the surface tension of soy oil is 0.0313 N/m. The surface tension of maltopentose is most likely an upper limit to the surface tension of our samples since maltopentose has a similar molecular weight but is more oxidized than our samples. Using an upper limit to the surface tension results in an upper limit to the simulated viscosities. For the Navier slip length, we used an upper limit to values reported in the literature.[10,11,20–22,12–19] An upper limit to the slip length also results in an upper limit to the

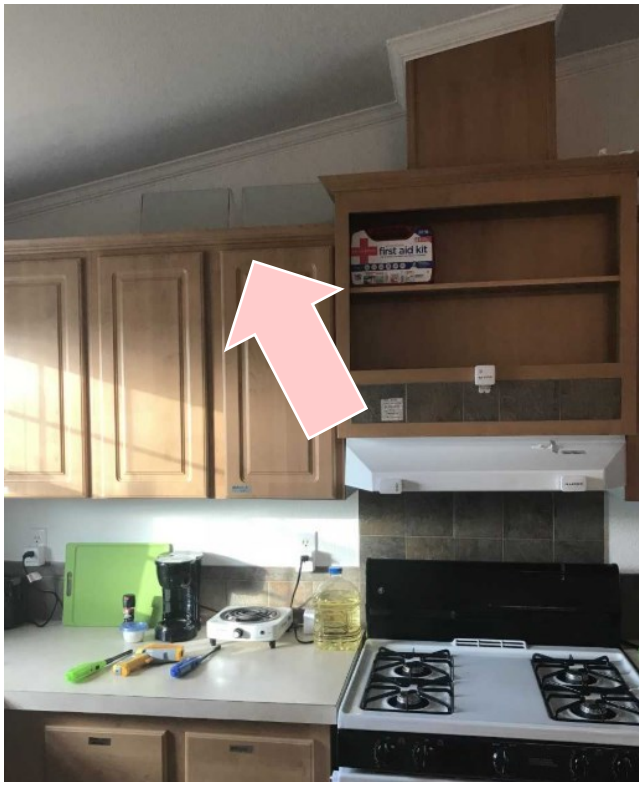

Figure S2. Glass plates deployed in the HOMEChem kitchen were located above the stove. Plates rested on the upper shelf and leaned against the back wall at a steep slant.

simulated viscosities.

The plates were located directly above the stove and were placed at as close to vertical as possible. As discussed in the manuscript, the majority of the mass is very similar to cooking organic aerosol. The other main type of activity during HOMEChem is cleaning.[23] No chlorine signals were observed in either the FT-ICR or the offline-AMS mass spectra for the solvent extract. Given the location of the plates, this suggests that the dominant mass contribution to this location in the house came from the cooking activities.

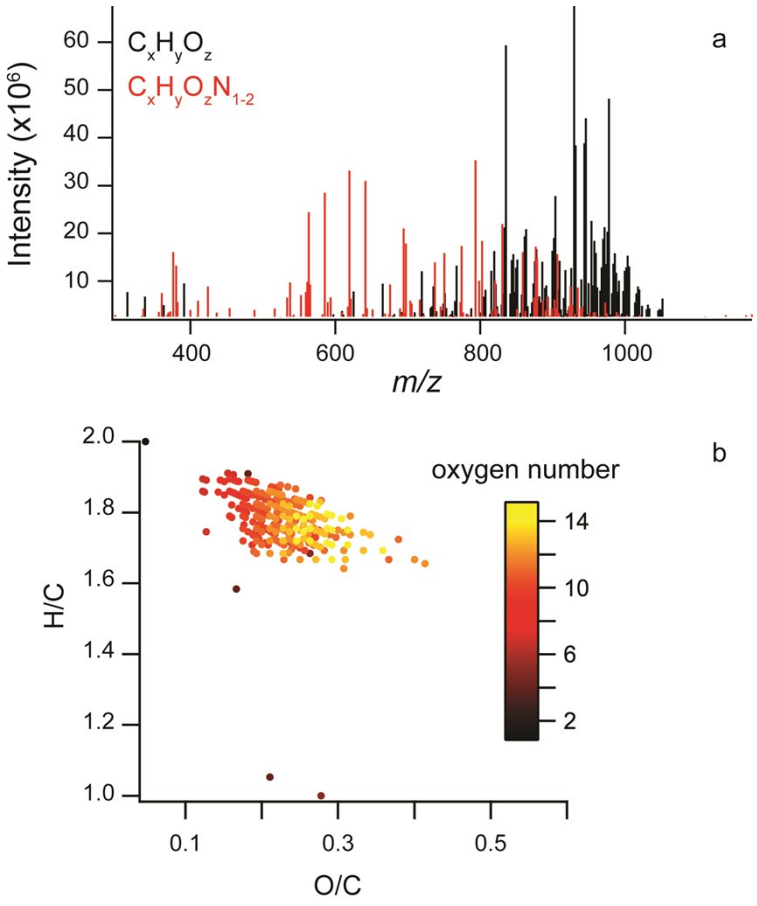

Figure S3. (a) ESI FT/ICR mass spectrum including both the CHO (black) and the CHON (red) containing ions. The CHO only ions are also in Figure 2. (b) Full Van Krevelen for Figure 2 in the manuscript for CHO only ions. Two ions had low H/C and were not included in Figure 2 to aid visualization.

Sensitivity simulations in glass transition temperature

Table S2 lists some triglyceride compounds that may exist in cooking oil.[24,25] Their measured T_g values are not available and we estimate T_g from measured melting temperatures (T_m) by applying the Boyer–Kauzmann rule of $T_g = g \times T_m$ with g = 0.70085 (±0.00375),[26] referred to as "estimated T_g" in this study. The calculated viscosities of triolein and tricaprylin applying the estimated T_g agree with their experimental viscosities,[25] indicating that the Boyer-Kauzmann rule works well to estimate T_g of triglycerides. The T_g predicted with the parameterization by DeRieux and Li et al. (2018)[27] could be by ~155 K – 245 K higher than the T_g estimated by the Boyer-Kauzmann rule, with higher DBE leading to larger overestimation.

To evaluate the effects of carbon-carbon double bonds on T_g prediction, we parameterize the overestimation of T_g by DeRieux and Li et al. (ΔT_g is the difference between the T_g predicted by DeRieux & Li and the estimated T_g) as a function of DBE and molar mass:

$$\Delta T_g = 2403.3 - 761.8017 \times \mathrm{DBE} - 2.5649 \times M + 0.8801 \times \mathrm{DBE} \times M \qquad \text{(Eq. S1)}$$

The coefficients in Eq. (S1) are obtained by fitting the ΔT_g in Table S2 with multilinear least squares analysis. The predicted ΔT_g values by Eq. S1 agree well with the T_g overestimation by DeRieux and Li et al. (Fig. S4b). Applying Eq. S1 in estimating T_g of CHO compounds in the surface extract results in a $T_{g,org}$ of 236 K. Note that Equation S1 based on only 6 triglyceride compounds is used as a sensitivity test evaluating the effects of DBE on T_g predictions of triglycerides. The parameterization based on a more comprehensive dataset considering the effects of structural information on viscosity predictions should be developed in future studies.

Table S2. Properties of six triglyceride compounds.

Species	Chemical formula	Molar mass (g	Experimental T_m (K)	T_g estimated from T_m	T_g predicted by	ΔT_g (T_g predicted by	Viscosity calculated from T_g	Experimental viscosity	DBE

		mol^{-1})		applying the Boyer-Kauzmann rule (K)	DeRieux & Li et al. (2018) (K)	DeRieux and Li minus estimated T_g) (K)	estimated from T_m (Pa s)	at 303 K (Pa s)	
Triolein[1]	$C_{57}H_{104}O_6$	885	269	188	425	237	0.25	0.0514[1]	6
Tripalmitin[1]	$C_{51}H_{98}O_6$	807	339	237	415	178	345.68		3
Tristearin[1]	$C_{57}H_{110}O_6$	892	345	242	428	186	822.77		3
Tricaprylin[1]	$C_{27}H_{50}O_6$	471	283	198	353	155	0.78	0.0165[1]	3
Tricaprin[2]	$C_{33}H_{62}O_6$	555	304	213	371	158	5.41		3
Trilinolenin[2]	$C_{57}H_{92}O_6$	873	250	175	420	245	0.07		12

[1]Valeri and Meirelles, 1997.

[2]Ceriani et al., 2007.

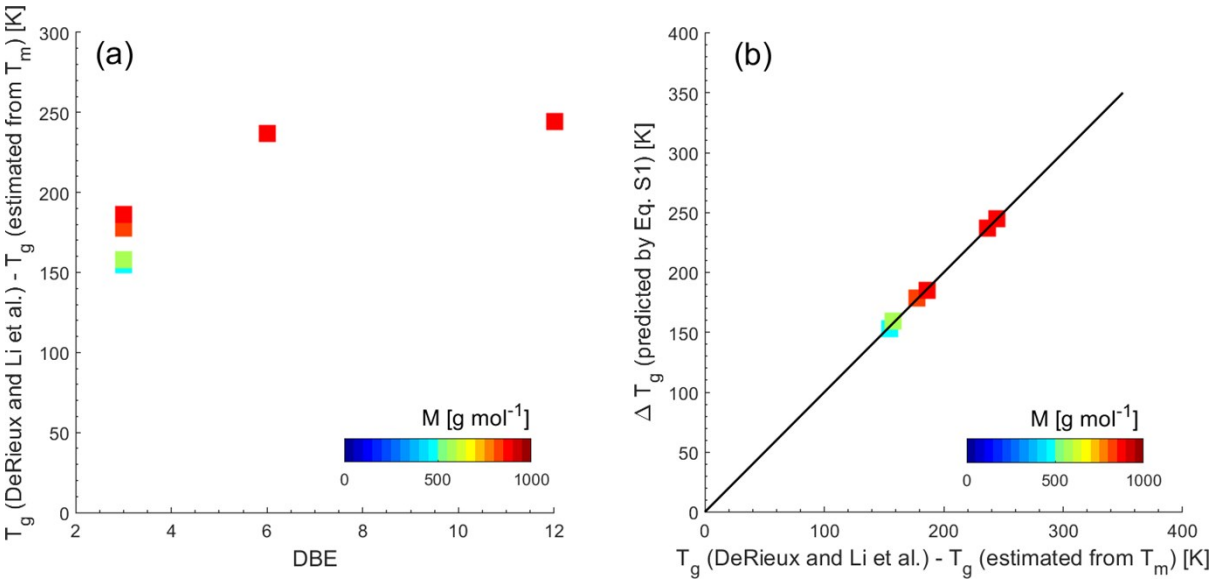

Figure S4. (a) T_g overestimation by DeRieux and Li et al. (2018) as a function of double bond equivalence (DBE) for compounds listed in Table S1. (b) Predicted T_g overestimation by DBE and molar mass (M, g mol^{-1}) (Eq. S1) plotted against the T_g overestimation by DeRieux and Li et al. (2018).

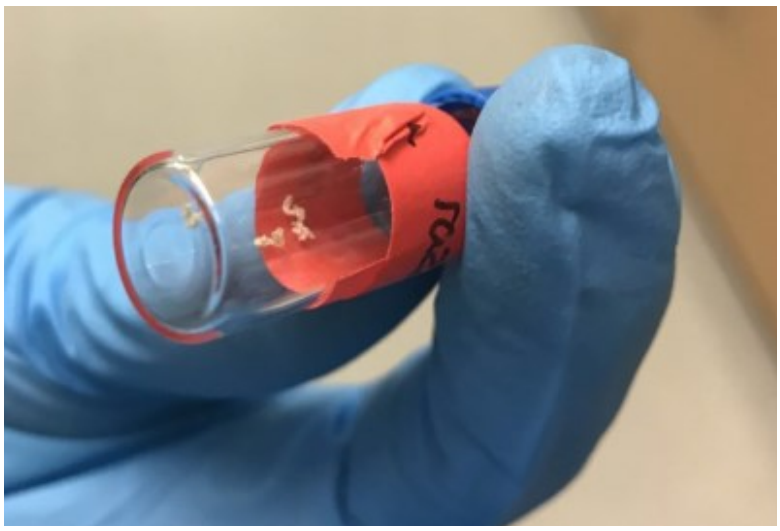

Figure S5. Material from the surface removed with a razor blade, the material is crumbly, not liquid like. This image is taken from a second razor scraping of the surface, no similar photograph was collected for the sample used to obtain the data in Or et al. (2020)[1]

References

(1) Lunderberg, D. M.; Kristensen, K.; Tian, Y.; Arata, C.; Misztal, P. K.; Liu, Y.; Kreisberg, N.; Katz, E. F.; DeCarlo, P. F.; Patel, S.; et al. Surface Emissions Modulate Indoor SVOC Concentrations through Volatility-Dependent Partitioning. *Environ. Sci. Technol.* **2020**, *54*, 6751–6760.

(2) Grayson, J. W.; Song, M.; Sellier, M.; Bertram, A. K. Validation of the poke-flow technique combined with simulations of fluid flow for determining viscosities in samples with small volumes and high viscosities. *Atmos. Meas. Tech.* **2015**, *8*, 2463–2472.

(3) Renbaum-Wolff, L.; Grayson, J. W.; Bateman, A. P.; Kuwata, M.; Sellier, M.; Murray, B. J.; Shilling, J. E.; Martin, S. T.; Bertram, A. K. Viscosity of a-pinene secondary organic material and implications for particle growth and reactivity. *Proc. Natl. Acad. Sci.* **2013**, *110* (20), 8014–8019.

(4) Grayson, J. W.; Zhang, Y.; Mutzel, A.; Renbaum-Wolff, L.; Böge, O.; Kamal, S.; Herrmann, H.; Martin, S. T.; Bertram, A. K. Effect of varying experimental conditions on the viscosity of α-pinene derived secondary organic material. *Atmos. Chem. Phys.* **2016**, *16*, 6027–6040.

(5) Grayson, J. W.; Evoy, E.; Song, M.; Chu, Y.; Maclean, A.; Nguyen, A.; Upshur, M. A.; Ebrahimi, M.; Chan, C. K.; Geiger, F. M.; et al. The effect of hydroxyl functional groups and molar mass on the viscosity of non-crystalline organic and organic-water particles.

Atmos. Chem. Phys. **2017**, *17*, 8509–8524.

(6) Song, M.; Liu, P. F.; Hanna, S. J.; Zaveri, R. A.; Potter, K.; You, Y.; Martin, S. T.; Bertram, A. K. Relative humidity-dependent viscosity of secondary organic material from toluene photo-oxidation and possible implications for organic particulate matter over megacities. *Atmos. Chem. Phys.* **2016**, *16*, 8817–8830.

(7) Song, M.; Liu, P. F.; Hanna, S. J.; Li, Y. J.; Martin, S. T.; Bertram, A. K. Relative humidity-dependent viscosities of isoprene-derived secondary organic material and atmospheric implications for isoprene-dominant forests. *Atmos. Chem. Phys.* **2015**, *15*, 5145–5159.

(8) Sahasrabudhe, S. N.; Rodriguez-Martinez, V.; Farkas, B. E. Density, viscosity, and surface tension of five vegetable oils at elevated temperatures: Measurement and modeling. *Int. J. Food Prop.* **2017**, *20* (S2), 51965–51981.

(9) Surface tension was determined with the ACD/Labs Percepta Platform-PhysChem Module, retrieved from ChemSpider http://www.chemspider.com/Chemical-Structure.18509779.html (accessed Dec 9, 2020).

(10) Baudry, J.; Charlaix, E.; Tonck, A.; Mazuyer, D. Experimental Evidence for a Large Slip Effect at a Nonwetting Fluid-Solid Interface. *Langmuir* **2001**, *17*, 5232–5236.

(11) Bhushan, B.; Wang, Y.; Maali, A. Boundary Slip Study on Hydrophilic, Hydrophobic, and Superhydrophobic Surfaces with Dynamic Atomic Force Microscopy. *Langmuir* **2009**, *25* (14), 8117–8121.

(12) Tretheway, D. C.; Meinhart, C. D. Apparent fluid slip at hydrophobic microchannel walls. *Phys. Fluids* **2002**, *14* (3), 9–12.

(13) Vinogradova, O. I.; Koynov, K.; Best, A.; Feuillebois, F.; Frumkin, A. N. Direct Measurements of Hydrophobic Slippage Using Double-Focus Fluorescence Cross-Correlation. *Phys. Rev. Lett.* **2008**, *102*, 1–4.

(14) Zhu, L.; Attard, P.; Neto, C. Reconciling Slip Measurements in Symmetric and Asymmetric Systems. *Langmuir* **2012**, *28*, 7768–7774.

(15) Cho, J.-H. J.; Law, B. M.; Rieutord, F. Dipole-dependent slip of Newtonian liquids at smooth solid hydrophobic surfaces. *Phys. Rev. Lett.* **2004**, *92* (16), 166102–166103.

(16) Churaev, N. V; Sobolev, V. D.; Somov, A. N. Slippage of Liquids over Lyophobic Solid Surfaces. *J. Colloid Interface Sci.* **1984**, *97* (2), 574–581.

(17) Cottin-Bizonne, C.; Cross, B.; Steinberger, A.; Charlaix, E. Boundary Slip on Smooth Hydrophobic Surfaces: Intrinsic Effects and Possible Artifacts. *Phys. Rev. Lett.* **2005**, *94*, 1–4.

(18) Cottin-Bizonne, C.; Jurine, S.; Baudry, J.; Crassous, J.; Restagno, F.; Charlaix, É. Nanorheology: An investigation of the boundary condition at hydrophobic and hydrophilic interfaces. *Eur. Phys. J. E* **2002**, *9* (1), 47–53.

(19) Craig, V. S. J.; Neto, C.; Williams, D. R. M. Shear-Dependent Boundary Slip in an Aqueous Newtonian Liquid. *Phys. Rev. Lett.* **2001**, *87* (5), 1–4.

(20) Jing, D.; Bhushan, B. Boundary Slip of Superoleophilic, Oleophobic, and Superoleophobic Surfaces Immersed in Deionized Water, Hexadecane, and Ethylene Glycol. *Langmuir* **2013**, *29*, 14691–14700.

(21) Joseph, P.; Tabeling, P. Direct measurement of the apparent slip length. *Phys. Rev. E* **2005**, *71*, 1–4.

(22) Mcbride, S. P.; Law, B. M. Viscosity-dependent liquid slip at molecularly smooth hydrophobic surfaces. *Phys. Rev.* **2009**, *80*, 06061.

(23) Farmer, D. K.; Vance, M. E.; Abbatt, J. P. D.; Abeleira, A.; Alves, M. R.; Arata, C.; Boedicker, E.; Bourne, S.; Cardoso-Saldã, F.; Corsi, R.; et al. Overview of HOMEChem: House Observations of Microbial and Environmental Chemistry. *Environ. Sci. Process. Impacts* **2019**, *21*, 1280–1300.

(24) Ceriani, R.; Gonçalves, C. B.; Rabelo, J.; Caruso, M.; Cunha, A. C. C.; Cavaleri, F. W.; Batista, E. A. C.; Meirelles, A. J. A. Group contribution model for predicting viscosity of fatty compounds. *J. Chem. Eng. Data* **2007**, *52* (3), 965–972.

(25) Valeri, D.; Meirelles, A. J. A. *Viscosities of Fatty Acids, Triglycerides, and Their Binary Mixtures*; 1997; Vol. 74.

(26) Koop, T.; Bookhold, J.; Shiraiwa, M.; Pöschl, U. Glass transition and phase state of organic compounds: dependency on molecular properties and implications for secondary organic aerosols in the atmosphere. *Phys. Chem. Chem. Phys.* **2011**, *13*, 19238–19255.

(27) Wong Derieux, W.-S.; Li, Y.; Lin, P.; Laskin, J.; Laskin, A.; Bertram, A. K.; Nizkorodov, S. A.; Shiraiwa, M. Predicting the glass transition temperature and viscosity of secondary organic material using molecular composition. *Atmos. Chem. Phys.* **2018**, *18*, 6331–6351.